Journal of Alloys and Compounds 515 (2012) 32–38

Contents lists available at SciVerse ScienceDirect

Journal of Alloys and Compounds

journal homepage: www.elsevier.com/locate/jallcom

Decomposition behaviour of $Mn(BH_4)_2$ formed by ball-milling $LiBH_4$ and $MnCl_2$

Ruixia Liu, Daniel Reed, David Book*

School of Metallurgy and Materials, University of Birmingham, Edgbaston, Birmingham B15 2TT, UK

ARTICLE INFO

Article history:
Received 12 July 2011
Received in revised form 11 October 2011
Accepted 12 October 2011
Available online 27 November 2011

Keywords:
Manganese borohydride
Hydrogen storage
Complex hydride
Mechanochemical synthesis
Thermogravimetric analysis
Raman spectroscopy

ABSTRACT

Manganese borohydride-based materials are of interest for hydrogen storage, as the $Mn(BH_4)_2$ compound has a theoretical hydrogen capacity of 9.53 wt.%. However, more needs to be known about the decomposition behaviour, in order to try to introduce reversibility. In this work, samples were prepared by ball-milling $xLiBH_4$ and $MnCl_2$ (where $x = 2$ or 3). The $Mn(BH_4)_2$ phase had XRD reflections consistent with the $P3_112$ structure proposed by Černý et al., and Raman spectroscopy indicted that the $[BH_4]^-$ units were in an ionic tetrahedral configuration. The $3LiBH_4 + MnCl_2$ sample contained excess $LiBH_4$ which exhibited an orthorhombic to hexagonal phase change at 93 °C indicating partial substitution of Cl^- for $[BH_4]^-$. Thermal decomposition of $Mn(BH_4)_2$ occurred between 130 and 181 °C for the $2LiBH_4 + MnCl_2$ sample and 105–145 °C for $3LiBH_4 + MnCl_2$, with the concurrent evolution of hydrogen and diborane. Analysis of the decomposition products shows the formation of amorphous boron, and the probable formation of manganese metal (deduced from the presence of manganese oxide in a sample subsequently exposed to air).

1. Introduction

Complex hydrides are of considerable interest for hydrogen storage in mobile applications due to their intrinsically high hydrogen contents [1]. Within this class of compound, alkali metal borohydrides exhibit the highest hydrogen densities, up to 18.5 wt.% and 121 kg H_2/m^3 for $LiBH_4$. However, $LiBH_4$ has a decomposition temperature greater than 400 °C and exhibits poor reversibility [2–4].

The inverse relationship between the thermal decomposition of single cation homoleptic borohydrides and the Pauling electronegativity of the cation has been empirically related through the enthalpy of formation [5]. Thermodynamic tuning through the formation of mixed cation borohydrides (e.g. $LiK(BH_4)_2$) was shown to be possible allowing borohydride based compounds to be selectively synthesised that have decomposition temperatures within the desired range for hydrogen storage applications [6,7].

Although there have been several attempts to synthesise homoleptic transition metal borohydrides, there has been little structural characterisation, with the exception of: $Zr(BH_4)_4$ [8,9], $Hf(BH_4)_4$ [10,11], $Y(BH_4)_3$ [12,13] and $Mn(BH_4)_2$ [14]. In-depth characterisation of the ball-milled zinc-based borohydride materials, showed that a number of different compounds can form depending on the alkali metal borohydride used as the precursor [15–17]. These studies also showed that there is a significant change in the decomposition temperatures and mechanisms depending on the alkali metal borohydride precursor used: decomposition temperatures ranged between 85 and 140 °C (with a mass loss >10 wt.%, however both diborane and hydrogen were evolved) [18].

Nakamori et al. ball-milled various metal chlorides with $LiBH_4$ to synthesise a series of transition metal borohydrides, M = Sc, Ti, V, Cr, Mn, Zn, Zr, Hf and Cu, and they assumed the formation of the homoleptic metal borohydrides [5,19–21]. The decomposition of the $Mn(BH_4)_2$ was shown to occur between 130 and 180 °C with a mass loss of 9.1 wt.% with the evolution of both hydrogen and diborane [19]. DFT calculations suggested that $Mn(BH_4)_2$ with a tetragonal *I-4m2* structure was the most energetically favourable [22], although an in-depth crystallographic and spectroscopic characterisation revealed a structure similar to that of α-$Mg(BH_4)_2$ with a trigonal crystal system with a space group of $P3_112$ that is stable between −180 and 175 °C [14]. This structure was also shown to form through mechanochemical and solvent synthesis with both 2:1 and 3:1 molar ratios of lithium borohydride to manganese chloride [23]. It has also been suggested that an amorphous phase of $LiMn(BH_4)_3$ is formed, although no direct evidence for this structure has been reported [22]. Thermal decomposition was reported between 135 and 155 °C with the release of 8.0 wt.% hydrogen and 120 °C with 7.4 wt.% H_2 [24]. Isothermal decomposition under 1 bar H_2 evolved 4.0 wt.% H_2 at 100 °C in 6 h and 4.5 wt.% H_2 at 120 °C in 2 h [25].

In order for $Mn(BH_4)_2$-based materials to have potential for practical use, the decomposition mechanism(s) need to be understood in detail so as to facilitate the development of reversible hydrogen sorption reaction pathways. The aim of this study is to

* Corresponding author. Tel.: +44 121 414 5213; fax: +44 121 414 5232.
E-mail address: d.book@bham.ac.uk (D. Book).

0925-8388/$ – see front matter © 2011 Elsevier B.V. All rights reserved.
doi:10.1016/j.jallcom.2011.10.067

prepare manganese borohydride compounds by mechanochemically reacting $LiBH_4$ and $MnCl_2$ in the molar ratios of 2:1 and 3:1, in order to investigate the structure and bonding of the resulting products and to characterise their thermal decomposition behaviour.

2. Experimental methods

2.1. Materials and synthetic method

Lithium borohydride ($LiBH_4$, 95%) and anhydrous manganese chloride ($MnCl_2$, 99.999%) were obtained from Sigma–Aldrich Company Ltd, and stored and handled in an argon-filled glovebox (MBraun Labstar) with the levels of water and oxygen kept below 0.1 ppm.

Mixtures of $LiBH_4$ and $MnCl_2$ powders, with 2:1 or 3:1 molar ratios, were put into a 250 ml stainless steel milling pot with stainless steel balls (12 mm diameter) with a ball-to-powder ratio of 32:1, and sealed with a Viton O-ring under argon. The mixture was milled using a Retsch PM400 Planetary Ball Mill at 175 rpm, for a total milling time of 6 h. In order to reduce the amount of heat generated, milling was carried out in 36 × 10 min durations separated by 10 min rest intervals.

2.2. XRD characterisation

The crystal properties of milled samples were investigated using a Bruker D8 Advance X-ray Diffractometer with Cu Kα radiation (λ = 0.154 nm). An Anton Parr XRK900 high-temperature sample cell was used to measure the temperature dependent properties under 3 bar flowing He (100 ml/min) and heated at 2 °C/min. TOPAS software [26] was used in the analysis of the measured XRD pattern.

2.3. Raman analysis

Raman spectra were obtained using a Renishaw inVia Raman Microscope with 488 nm excitation laser (2 mW power on the sample). A microscope objective was used to focus the laser beam onto the sample with a spot-diameter of about 50 μm. An Instec HCS621V sample cell stage was used to measure temperature-dependent Raman spectra, by heating samples at 2 °C/min in 1 bar Ar flowing at 100 ml/min.

2.4. FTIR analysis

Fourier transform infrared (FTIR) spectra were obtained using a Thermo 8700 spectrometer fitted with a Specac "Golden Gate" ATR sample cell. The spectral resolution of 0.48 cm^{-1} was used for FTIR measurements. The bench was purged with nitrogen for 30 min prior to collection of the background to obtain a constant carbon dioxide and water concentrations within the spectrometer, allowing inert loading without the need for separate backgrounds before each spectrum.

2.5. Thermal analysis

The thermal decomposition behaviour of the milled mixtures was investigated by thermogravimetric analysis (TGA, Netzsch TG209) with the exhaust gases analysed by mass spectrometry (MS, Hiden Analytical HAL IV). Approximately 10–15 mg of sample was heated at 2 °C/min under 1.5 bar flowing Ar (40 ml/min) in an alumina crucible. The MS was set up to measure the concentrations of H_2 ($m/z = 2$), and B_2H_6 ($m/z = 26$). However, it should be noted that the value for the concentration of B_2H_6 will depend on the experimental setup: in this study it is likely that a proportion of any B_2H_6 evolved may be deposited onto the surfaces of the connecting pipe between the TGA and MS, affecting the concentration values for B_2H_6. Differential scanning calorimetry (DSC, Netzsch DSC204HP) was performed on approximately 10 mg samples in an Al crucible heated at 2 °C/min under 4 bar flowing Ar (100 ml/min).

3. Results and discussion

3.1. Characterisation of the milled material

XRD measurements, Fig. 1, show diffraction peaks attributed to LiCl and the $P3_112$ structure of $Mn(BH_4)_2$ proposed by Černý et al. [14] for both $2LiBH_4 + MnCl_2$ and $3LiBH_4 + MnCl_2$ samples. For the $2LiBH_4 + MnCl_2$ sample the metathesis reaction may be given by (Eq. (1)):

$$2LiBH_4 + MnCl_2 \rightarrow Mn(BH_4)_2 + 2LiCl \quad (1)$$

Therefore, excess $LiBH_4$ may be expected for the $3LiBH_4 + MnCl_2$ sample. However, this was not observed by XRD; this may be due to the comparatively small concentration of $LiBH_4$. The lattice parameters of $Mn(BH_4)_2$ were found to be $a = 10.48(1)$ Å and $c = 10.82(1)$ Å for the $2LiBH_4 + MnCl_2$ sample and $a = 10.42(1)$ Å and $c = 10.81(1)$ Å

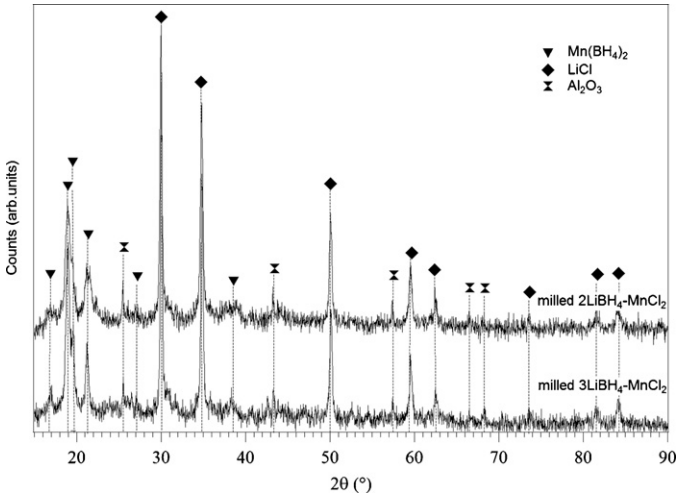

Fig. 1. XRD patterns of $xLiBH_4 + MnCl_2$ ($x = 2$ or 3) samples ball-milled for 6 h.

for the $3LiBH_4 + MnCl_2$ sample, using the structure proposed by Černý et al. [14]. The reduction in lattice parameter a could be due to the substitution of some of the $[BH_4]^-$ anions by Cl^- anions present in the mixture. Such a substitution was discussed as a possible explanation for the decrease in volume during heating between −183 and 127 °C by Černý et al. [14]

Raman spectroscopy can be used to identify the nature of the bonding of the borohydride to the metal centre, as ionic, mono-, bi- and tridentate configurations have characteristic modes [27]. Fig. 2 shows the room temperature Raman spectra of the milled products (with $LiBH_4$ as a reference), with peak positions summarised in Table 1. For both samples, the spectra are dominated by five fundamental Raman vibrations, B–H bending modes occurring at 1092/1094, 1155, 1172/1175 and 1353 cm^{-1}, and B–H stretch at 2269/2270 cm^{-1} with combination modes at 2155/2157 and 2460 cm^{-1}, of which the modes at 1172–1175 and 1353 cm^{-1} are not observed for as received $LiBH_4$. The product of the $2LiBH_4 + MnCl_2$ has a spectrum consistent with an ionic $[BH_4]^-$, although the B–H stretching region (2100–2400 cm^{-1}) is moved to lower Raman shifts compared to $LiBH_4$. This may have been induced by both a lengthening of the B–H bond and also the change in the force constant due to the interaction with the divalent Mn ion. The spectrum from the $3LiBH_4 + MnCl_2$ sample exhibits the same ionic modes as the $2LiBH_4 + MnCl_2$ sample with additional modes

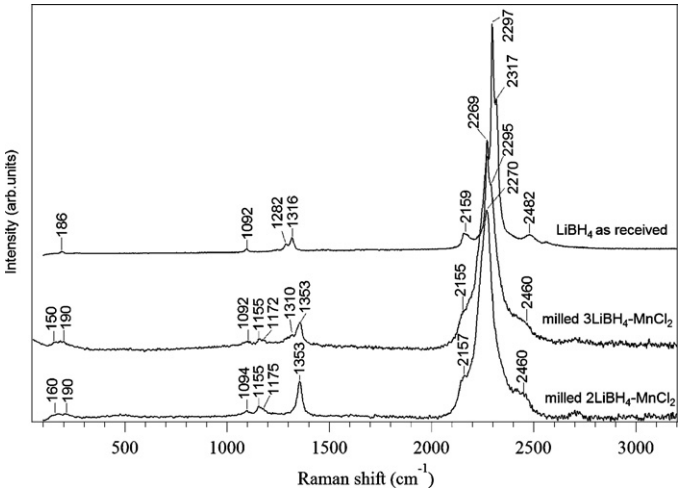

Fig. 2. Raman spectra of $xLiBH_4 + MnCl_2$ ($x = 2$ or 3) samples ball-milled for 6 h, with $LiBH_4$ as a reference.

Table 1
Summary of Raman shift values (cm^{-1}) of the resulting products from two ball-milled $LiBH_4 - MnCl_2$ mixtures, compared to values from the literature for $LiBH_4$ and $Mn(BH_4)_2$.

$LiBH_4$ [28]	$LiBH_4$ (this work)	$2LiBH_4 - MnCl_2$ [14]	(This work)		Assignment
			$2LiBH_4 - MnCl_2$	$3LiBH_4 - MnCl_2$	
189	186		160–190	150–190	
255	–		–	–	External mode
283	–		–	–	
1090	1092 w	1102	1094 vw	1092 vw	
1099	–	1164	1155 w	1155 w	
–	–	1175	1175 s	1172 sh	
1235	–		–	–	B–H bending modes
1286	1282 sh		–	1281	
1316	1316 m		–	1310 sh	
–		1359	1353 s	1353 m	
2157	2159 m	2161	2157 w	2155 w	
2177	–		–	–	
2275	2269 sh	2271	2270 vs	2269 vs	
2301	2297 vs		–	2295 sh	
2321	2317 sh		–	–	B–H stretching modes
2391	–		–	–	
2491	2482 w		2460 w	2460	
2572	–		–	–	

(1310 and 2295 cm^{-1}) confirming the presence of excess $LiBH_4$ in this sample. The absence of extensive splitting of the B–H bending modes (1000–1330 cm^{-1}) indicates that the $[BH_4]^-$ ions occupy relatively high-symmetry sites with all the $[BH_4]^-$ ions existing in similar environments.

In addition, FTIR measurements showed vibrations at 2230, 1352, 1203, 1091 cm^{-1} in both samples, which may be associated with the $[BH_4]^-$ tetrahedrons of $Mn(BH_4)_2$, as shown in Fig. 3. Vibrations at 2305, 1092 and 964 cm^{-1} confirm the presence of excess $LiBH_4$ in the $3LiBH_4 + MnCl_2$ sample.

These XRD, Raman and FTIR results appear to confirm that the metathesis reaction has taken place according to Eq. (1).

3.2. Thermal analysis

There are many thermal decomposition pathways possible for metal borohydrides [28]. Many involve the evolution of hydrogen (and/or diborane) to leave metallic manganese (Eqs. (2) and (3)), boron (Eq. (2)), metal boride (Eq. (4)) or a borane (e.g. dodecaborane $[B_{12}H_{12}]^{2-}$) as the solid decomposition product(s). The most probable decomposition reactions for $Mn(BH_4)_2$ (or a combination, thereof), are shown in Eqs. (2)–(4).

$$Mn(BH_4)_2 \rightarrow Mn + 2B + 4H_2 \quad (2)$$

$$Mn(BH_4)_2 \rightarrow Mn + H_2 + B_2H_6 \quad (3)$$

$$Mn(BH_4)_2 \rightarrow MnB_2 + 4H_2 \quad (4)$$

It is also noted that manganese boride can exist in a number of other forms: MnB_4, Mn_3B_4, MnB and Mn_2B [29]. The expected mass loss for Eqs. (2) and (4) would be 9.53 wt.% (4.76 or 4.22 wt.% for the ball-milled mixtures $2LiBH_4 + MnCl_2$ and $3LiBH_4 + MnCl_2$, respectively). A mass loss of 35.08 wt.% would be expected from Eq. (3) (17.52 and 15.53 wt.% for mixtures $2LiBH_4 + MnCl_2$ and $3LiBH_4 + MnCl_2$, respectively).

Thermogravimetric analysis of the $2LiBH_4 + MnCl_2$ sample (Fig. 4) shows the onset of decomposition is 130 °C and is complete by 181 °C with a mass loss of 8.4 ± 0.2 wt.%. This mass loss is not consistent with any of the single proposed mechanisms above. Mass spectrometry (Fig. 4) shows that there is a concurrent evolution of hydrogen and trace diborane with an onset of 133 °C, reaching a peak at 148 °C. The low intensity of diborane is due to the experimental set-up: deposits of borate observed on the interconnecting pipe work, suggests that a significant amount of dibornae does not reach the mass spectrometer gaseous borane compounds other then diborane were not detected by MS in this study. In addition, the MS shows a second, smaller hydrogen evolution peak at

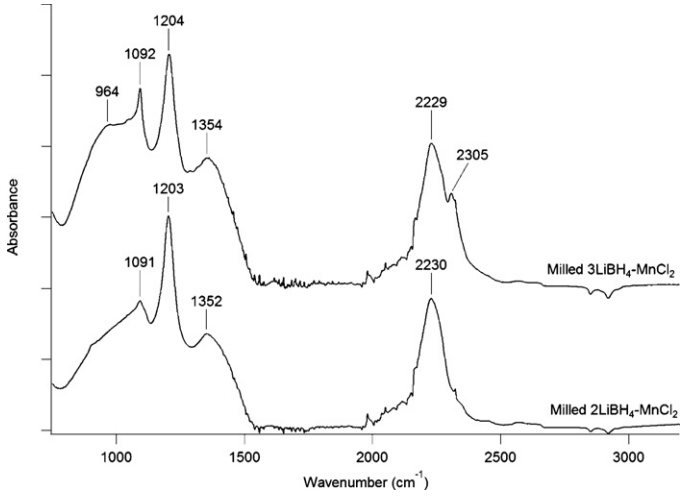

Fig. 3. FTIR spectra of $xLiBH_4 + MnCl_2$ ($x = 2$ or 3) samples ball-milled for 6 h.

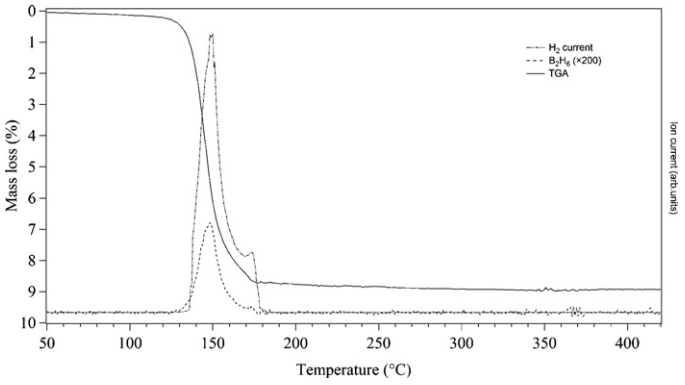

Fig. 4. TGA profile for $2LiBH_4 + MnCl_2$ heated at 2 °C/min in 1.5 bar Ar flowing at 40 ml/min, coupled with MS data for evolved H_2 and B_2H_6 gases.

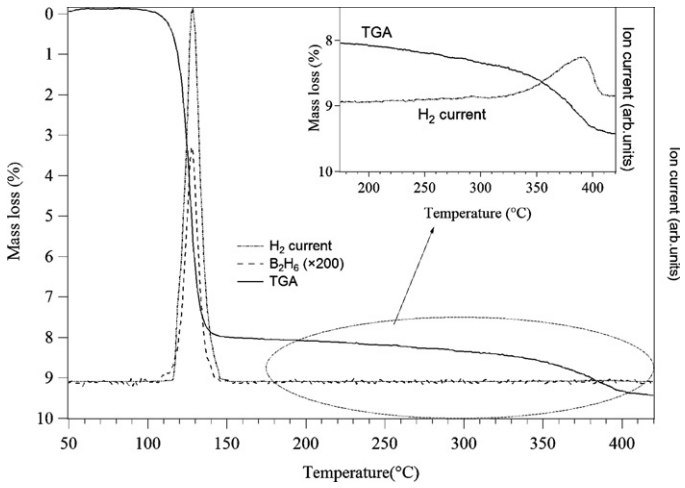

Fig. 5. TGA profile for $3LiBH_4 + MnCl_2$ heated at 2 °C/min in 1.5 bar Ar flowing at 40 ml/min, coupled with MS data for evolved H_2 and B_2H_6 gases. Inset figure shows an expanded region between 200 and 420 °C.

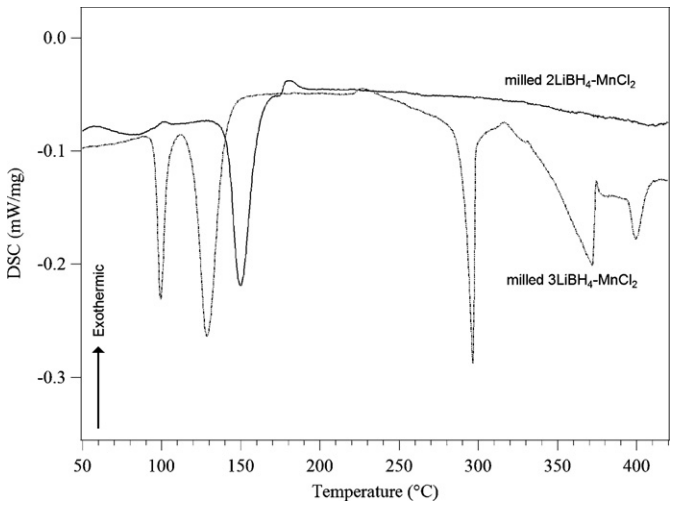

Fig. 6. DSC profiles of milled $2LiBH_4 - MnCl_2$ and $3LiBH_4 - MnCl_2$ samples heated in 3 bar Ar flowing at 100 ml/min.

around 170 °C corresponding to a small change in the gradient of the TGA. The presence of a second decomposition step indicates that either there are two distinct mechanisms for decomposition or that the decomposition involves a two-step process proceeding via an intermediate species.

TGA of the $3LiBH_4 + MnCl_2$ sample (Fig. 5) has two distinct regions of decomposition. Firstly the decomposition between 105 and 145 °C with a mass loss of 8.1 ± 0.2 wt.% is attributed to the decomposition of $Mn(BH_4)_2$, while the second decomposition of 0.9 ± 0.2 wt.% between 320 and 410 °C is in the range consistent with a 9 wt.% (1.0 wt.% of total system) decomposition of the residual $LiBH_4$ [2]. The 25 °C reduction in the decomposition temperature of $Mn(BH_4)_2$ could be due to: a change in decomposition mechanism; a change in microstructure brought about by a different milling behaviour, due to the presence of the remnant $LiBH_4$; and/or some form of 'catalytic' effect of the $LiBH_4$.

MS of the $3LiBH_4 + MnCl_2$ sample shows the concurrent evolution of hydrogen and diborane accompanying the mass loss observed on the TGA between 105 and 145 °C. Unlike the $2LiBH_4 + MnCl_2$ sample, no second hydrogen desorption MS peak was observed. The only gas evolved between 320 and 410 °C is hydrogen, which is consistent with the decomposition of $LiBH_4$ [3].

Differential Scanning Calorimetry of the $2LiBH_4 + MnCl_2$ sample (Fig. 6) shows a number of peaks. The most significant of these is the endothermic peak between 130 and 170 °C, which corresponds to the mass loss observed on the TGA (Fig. 4).

DSC of the $3LiBH_4 + MnCl_2$ sample shows several peaks. The lowest in temperature occurs with an onset of 93 °C and is attributed to the orthorhombic to hexagonal phase change in the excess $LiBH_4$, this value is significantly lower than pure $LiBH_4$ (118 °C) due to possible Cl^- substitution for $[BH_4]^-$ ions [30,31]. This substitution may account for the reduced mass loss observed for $LiBH_4$ using TGA. An endotherm with an onset of 285 °C is due to the melting of $LiBH_4$, there then follows a series of peaks typical of the decomposition of $LiBH_4$ [32]. The decomposition of $Mn(BH_4)_2$ occurs between 113 and 150 °C, indicating a single decomposition step consistent with the TGA and MS results (Fig. 5).

3.3. Decomposition behaviour

In situ XRD heating from room temperature to 400 °C in an inert atmosphere was performed to monitor the change in crystalline phases with temperature. Samples were loaded in Al_2O_3 crucibles and therefore small reflections due to the crucible are observed in all patterns. Fig. 7 shows the patterns from the $2LiBH_4 + MnCl_2$ sample. At room temperature reflections due to the reaction products LiCl and $Mn(BH_4)_2$ are observed. Between 150 and 160 °C the reflections due to $Mn(BH_4)_2$ are no longer present due to the decomposition of this compound, however, no new reflections are observed, indicating the formation of amorphous manganese and boron species. No phases apart from LiCl are observed above 160 °C.

Fig. 8 shows the XRD patterns for decomposition of the $3LiBH_4 + MnCl_2$ sample. At room temperature all the reflections are attributed to LiCl and $Mn(BH_4)_2$, upon heating, reflections due to the hexagonal phase of $LiBH_4$ are observed between 120 and 300 °C. Decomposition of $Mn(BH_4)_2$ occurs between 130 and 150 °C with only a slight trace observed at 140 °C, correlating with the TGA and DSC results (Figs. 4 and 6). As with the $2LiBH_4 + MnCl_2$ sample no reflections are observed for the decomposition products. Above 320 °C a number of unknown phases are observed; these peaks are not consistent with MnH, LiH, $Li_2B_{12}H_{12}$, $Li_2B_{10}H_{10}$, or Li_2MnCl_4 [33–35]. However, we have tentatively assigned them as three separate phases. Unknown phase I is observed with reflections at 13.1, 19.3 and 26.4° 2θ and unknown phase II with reflections at 20.2, 27.4 and 27.9° 2θ. Unknown phase I is no longer present above 380 °C whereas unknown phase II is stable to 400 °C. Two reflections in unknown phase I (13.1° and 19.3°) and two in unknown

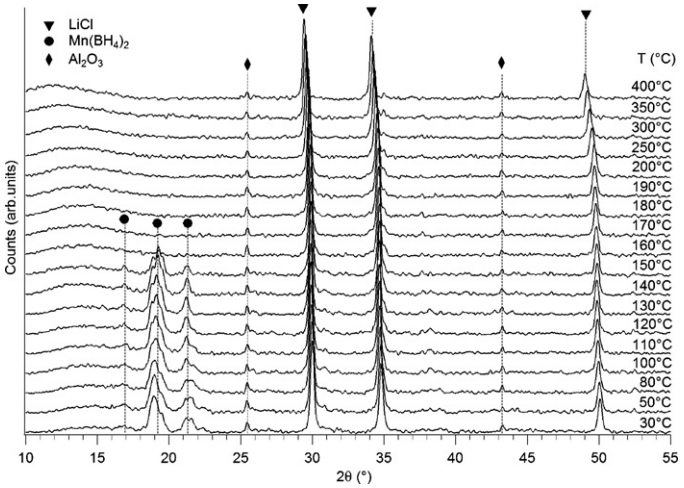

Fig. 7. In situ XRD patterns of milled $2LiBH_4 - MnCl_2$ heated at 2 °C/min in 4 bar He flowing at 100 ml/min.

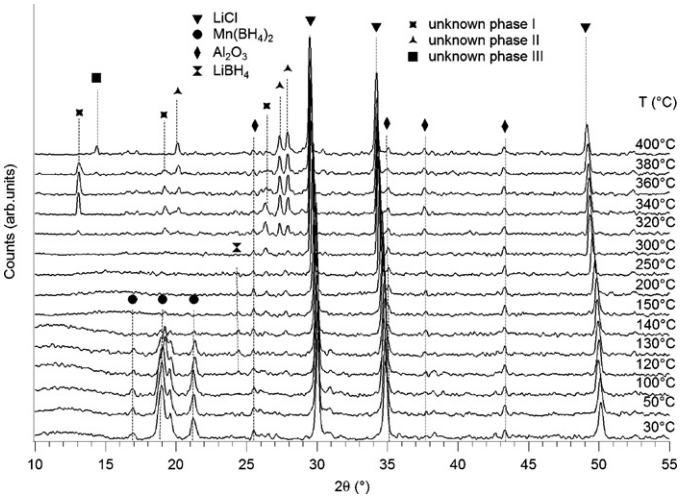

Fig. 8. In situ XRD patterns of milled $3LiBH_4 - MnCl_2$ heated at 2 °C/min in 4 bar He flowing at 100 ml/min.

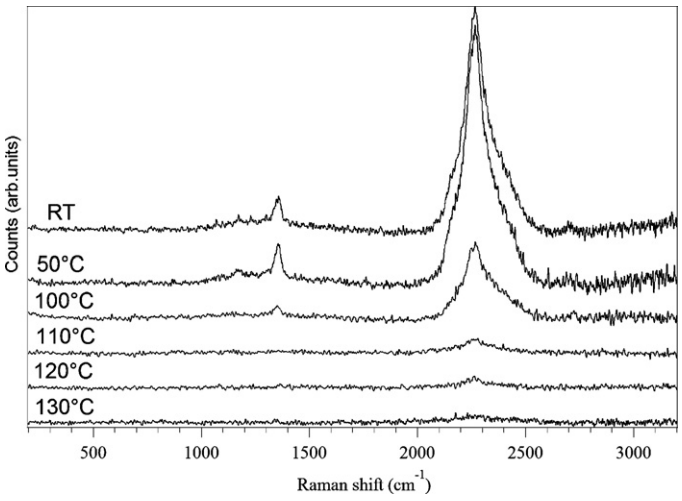

Fig. 10. In situ Raman spectra of milled $3LiBH_4 - MnCl_2$ heated at 2 °C/min in 1 bar Ar flowing at 100 ml/min.

phase II (20.2° and 27.9°) are similar to reflections reported for two unknown phases (13.2°, 19.7° and 19.9°, 27.9°) during the decomposition of $LiBH_4$ [36]. However, there are a number of additional high intensity reflections for the unknown phases in [36] that are not observed in Fig. 8. At 400 °C unknown phase III is observed as a single reflection at 14.4° 2θ. The temperature region from 320 to 400 °C is consistent with the decomposition temperature range of $LiBH_4$ shown in Figs. 5 and 6, where a broad hydrogen release takes place together with two endothermic DSC peaks at 320–380 °C and 390–420 °C. Thus, these unknown phases are likely to be the decomposition products of $LiBH_4$ forming within, and/or reacting with, the mixture of decomposed $Mn(BH_4)_2$ phases [37,38].

In situ Raman spectroscopy of the $2LiBH_4 + MnCl_2$ (Fig. 9) shows a reduction in intensity of the B–H stretching modes at 120 °C with no B–H stretching or bending modes present at 150 °C this corresponds well with the thermal decomposition of $Mn(BH_4)_2$ with the loss of H_2 and B_2H_6.

The reduction in B–H stretch intensity of the $3LiBH_4 + MnCl_2$ sample occurs at 100 °C with complete removal of B–H bonding above 110 °C as the $Mn(BH_4)_2$ decomposes (Fig. 10). There are no bands observed for the remaining $LiBH_4$, this is believed to be due to the small concentration (approx. 11.4 wt.%) in the sample.

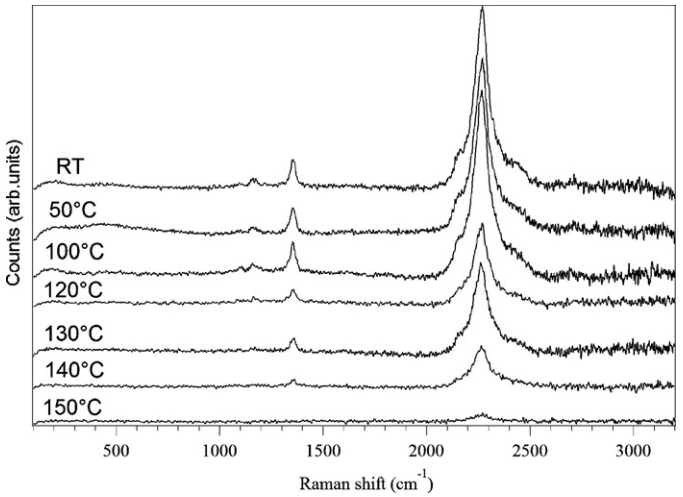

Fig. 9. In situ Raman spectra of milled $2LiBH_4 - MnCl_2$ heated at 2 °C/min in 1 bar Ar flowing at 100 ml/min.

The absence of manganese boride indicates that the decomposition reaction has not occurred via Eq. (4) or resulted in the formation of a similar manganese boride.

Ex situ Raman and FTIR measurements were carried out on milled $2LiBH_4 + MnCl_2$ sample that had been heated to 200, and then subsequently exposed to air for 5 min at room temperature. Fig. 11 shows the Raman spectra of decomposed products for milled $2LiBH_4 + MnCl_2$ sample; a sharp band at 660 cm^{-1} is observed for all the samples, which is attributed to manganese oxide (Mn_3O_4) [39,40]. This result indirectly indicates that manganese is formed as one of the decomposition products of the milled $xLiBH_4 + MnCl_2$ samples.

Fig. 12 shows the FTIR spectra of $2LiBH_4 + MnCl_2$ sample after heating. The sample heated to 200 °C shows bands attributed to Mn_3O_4 at 943 and 1039 cm^{-1} and bands at 1245 and 1331 cm^{-1} associated with B–B vibrations attributed to amorphous boron.

The act of mechanically milling lithium borohydride and manganese chloride resulted in the formation of manganese borohydride and lithium chloride as per Eq. (1). Investigations into the thermal decomposition of manganese borohydride occurred by a two step mechanism resulting in the evolution of hydrogen and diborane (9:1 molar ratio) leaving residual manganese and boron. It therefore seems likely that the thermal decomposition reaction of $Mn(BH_4)_2$ proceeds via a combination of Eqs. (2) and (3) with a 2:1 ratio as shown in Eq. (5):

$$3Mn(BH_4)_2 \rightarrow 3Mn + 4B + B_2H_6 + 9H_2 \quad (5)$$

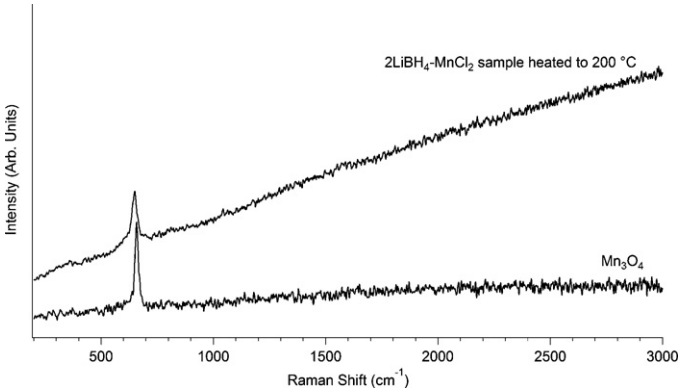

Fig. 11. Ex situ room temperature Raman spectra of $2LiBH_4 - MnCl_2$ sample heated to 200 °C under Ar and then exposed to air for 5 min.

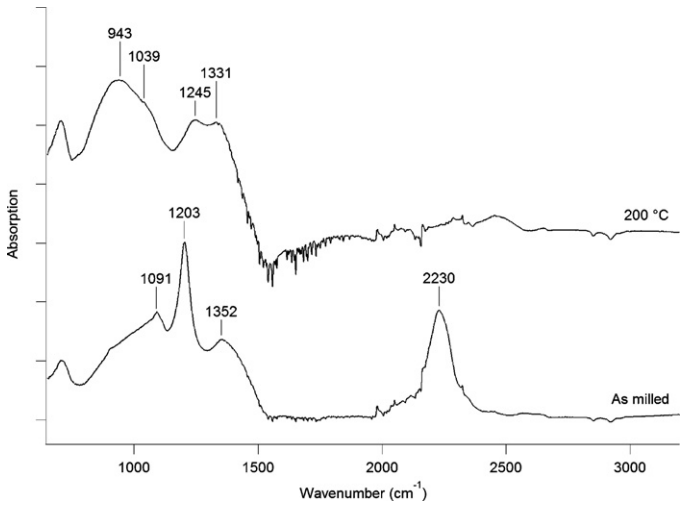

Fig. 12. Ex situ room temperature FTIR spectra of milled $2LiBH_4 - MnCl_2$ of samples heated to 200 °C under Ar and then exposed to air for 5 min.

where the theoretical mass loss is calculated as 8.9 wt.% in $Mn(BH_4)_2 + 2LiCl$ mixture, which matches the experimental data (8.4 wt.%). It is not clear why Mn is not observed by XRD (Figs. 7 and 8) in this study, unless it is possibly in the form of finely dispersed nanoscale grains. Alternatively, an amorphous Mn–B compound, such as MnB, MnB_2,or Mn_3B_4 [41] would explain the absence of Mn X-ray peaks. However, the Mn–B vibrations in the Raman and FT-IR spectra are absent (Figs. 11 and 12).

The $3LiBH_4 + MnCl_2$ sample has excess $LiBH_4$ within the sample that does not appear to be involved in the thermal decomposition of manganese borohydride. The excess lithium borohydride decomposes between 320 and 410 °C with the formation of several unidentified phases.

Recombination was attempted on a decomposed (heated to 200 °C under 1.5 bar Ar flowing at 40 ml/min) $2LiBH_4 + MnCl_2$ sample. It was heated to 200 °C in 100 bar H_2 flowing at 100 ml/min, without any isothermal dwell. However, no endo/exothermic DSC peaks were observed during heating in hydrogen, and subsequently, no mass loss or gas desorption was observed when the treated sample was heated in flowing argon on a TGA coupled to a mass spectrometer. This indicates that there is no reversibility within this system, under these conditions.

4. Conclusions

Manganese borohydride was successfully synthesised by mechanochemical milling of $xLiBH_4 + MnCl_2$ ($x = 2$ or 3) mixtures. Analysis of the milled materials shows the presence of crystalline LiCl and $Mn(BH_4)_2$ in both samples, plus excess $LiBH_4$ in the $3LiBH_4 + MnCl_2$ sample. This shows that the reaction occurred via the metathesis reaction shown in Eq. (1).

Thermal decomposition of $Mn(BH_4)_2$ occurs between 130 and 181 °C for the $2LiBH_4 + MnCl_2$ sample and from 105 to 145 °C for $3LiBH_4 + MnCl_2$ resulting in the concurrent evolution of hydrogen and diborane. A second TGA decomposition step may possibly indicate two mechanisms for decomposition and/or the formation of an intermediate phase.

Analysis of the final decomposition products by FTIR and Raman shows the formation of amorphous boron, and the absence of any Mn–B vibrations. In addition, the probable formation of manganese metal is deduced from the presence of manganese oxide in a sample which was deliberately exposed to air. The overall reaction is most likely:

$$Mn(BH_4)_2 \rightarrow Mn + (4/3)B + (1/3)B_2H_6 + 3H_2$$

The $3LiBH_4 + MnCl_2$ sample has excess $LiBH_4$ which goes through the orthorhombic to hexagonal phase change at 93 °C indicating partial substitution of Cl^- for $[BH_4]^-$ within the lattice. Melting occurs at 285 °C followed by a series of reactions as $LiBH_4$ interacts with the decomposition products of $Mn(BH_4)_2$ with the evolution of H_2 and the formation of three as yet unidentified phases (320–400 °C)

Acknowledgements

The authors gratefully acknowledge support from the AWM Birmingham Science City Hydrogen Energy project and the EPSRC SUPERGEN UK Sustainable Hydrogen Energy Consortium (EP/E040071/1).

References

[1] S.I. Orimo, Y. Nakamori, J.R. Eliseo, A. Züttel, C.M. Jensen, Chem. Rev. 107 (2007) 4111–4132.
[2] A. Züttel, S. Rentsch, P. Fischer, P. Wenger, P. Sudan, P. Mauron, C. Emmenegger, J. Alloys Compd. 356 (2003) 515–520.
[3] A. Züttel, P. Wenger, S. Rentsch, P. Sudan, P. Mauron, C. Emmenegger, J. Power Sources 118 (2003) 1–7.
[4] S. Orimo, Y. Nakamori, G. Kitahara, K. Miwa, N. Ohba, S. Towata, A. Züttel, J. Alloys Compd. 404 (2005) 427–430.
[5] Y. Nakamori, K. Miwa, A. Ninomiya, H.W. Li, N. Ohba, S.I. Towata, A. Züttel, S.I. Orimo, Phys. Rev. B 74 (2006) 045126.
[6] H.W. Li, S. Orimo, Y. Nakamori, K. Miwa, N. Ohba, S. Towata, A. Züttel, J. Alloys Compd. 446–447 (2007) 315–318.
[7] E.A. Nickels, M.O. Jones, W.I.F. David, S.R. Johnson, R.L. Lowton, M. Sommariva, P.P. Edwards, Angew. Chem. Int. Ed. 47 (2008) 2817–2819.
[8] P.H. Bird, M.R. Churchill, Chem. Commun. (1967) 403–1403.
[9] J.O. Jensen, Vib. Spectrosc. 31 (2003) 227–250.
[10] R.W. Broach, I.S. Chuang, T.J. Marks, J.M. Williams, Inorg. Chem. 22 (1983) 1081–1084.
[11] J.O. Jensen, Spectrochim. Acta. A. 59 (2003) 379–392.
[12] T. Sato, K. Miwa, Y. Nakamori, K. Ohoyama, H.W. Li, T. Noritake, M. Aoki, S.I. Towata, S.I. Orimo, Phys. Rev. B 77 (2008) 104114.
[13] D. Ravnsbæk, Y. Filinchuk, R. Cerny, M.B. Ley, D. Haase, H.J. Jakobsen, J. Skibsted, T.R. Jensen, Inorg. Chem. 49 (2010) 3801–3809.
[14] R. Cerny, N. Penin, H. Hagernann, Y. Filinchuk, J. Phys. Chem. C 113 (2009) 9003–9007.
[15] D. Ravnsbæk, Y. Filinchuk, Y. Cerenius, H.J. Jakobsen, F. Besenbacher, J. Skibsted, T.R. Jensen, Angew. Chem. Int. Ed. 48 (2009) 6659–6663.
[16] D.B. Ravnsbæk, L.H. Sørensen, Y. Filinchuk, D. Reed, D. Book, H.J. Jakobsen, F. Besenbacher, J. Skibsted, T.R. Jensen, Eur. J. Inorg. Chem. 2010 (2010) 1608–1612.
[17] D.B. Ravnsbæk, C. Frommen, D. Reed, Y. Filinchuk, M. Sørby, B.C. Hauback, H.J. Jakobsen, D. Book, F. Besenbacher, J. Skibsted, T.R. Jensen, J. Alloys Compd. 509S (2011) S698–S704.
[18] E. Jeon, Y. Cho, J. Alloys Compd. 422 (2006) 273–275.
[19] Y. Nakamori, H.W. Li, K. Kikuchi, M. Aoki, K. Miwa, S. Towata, S. Orimo, J. Alloys Compd. 446–447 (2007) 296–300.
[20] Y. Nakamori, H.W. Li, M. Matsuo, K. Miwa, S. Towata, S. Orimo, J. Phys. Chem. Solids 69 (2008) 2292–2296.
[21] Y. Nakamori, H.W. Li, K. Miwa, S. Towata, S. Orimo, Mater. Trans. 47 (2006) 1898–1901.
[22] P. Choudhury, V.R. Bhethanabotla, E. Stefanakos, J. Phys. Chem. C 113 (2009) 13416–13424.
[23] G. Severa, H. Hagemann, M.s. Longhini, J.W. Kaminski, T.A. Wesolowski, C.M. Jensen, J. Phys. Chem. C 114 (2010) 15516–15521.
[24] P. Choudhury, S.S. Srinivasan, V.R. Bhethanabotla, Y. Goswami, K. McGrath, E.K. Stefanakos, Int. J. Hydrogen Energy 34 (2009) 6325–6334.
[25] R.A. Varin, L. Zbroniec, Int. J. Hydrogen Energy 35 (2010) 3588–3597.
[26] A.A. Coelho, TOPAS General Profile and Structure Analysis Softwere for Powder Diffraction Data, Bruker AXS, Karlsruhe, Germany, 2004.
[27] T.J. Marks, J.R. Kolb, Chem. Rev. 77 (1977) 263–293.
[28] D. Reed, D. Book, Curr. Opin. Solid State Mater. Sci. 15 (2011) 62–72.
[29] W.H. Sun, Y. Du, S.H. Liu, B.Y. Huang, C. Jiang, J. Phase Equilib. Diffus. 31 (2010) 357–364.
[30] L.M. Arnbjerg, D.B. Ravnsbaek, Y. Filinchuk, R.T. Vang, Y. Cerenius, F. Besenbacher, J.E. Jorgensen, H.J. Jakobsen, T.R. Jensen, Chem. Mater. 21 (2009) 5772–5782.
[31] L. Mosegaard, B. Moller, J.E. Jorgensen, Y. Filinchuk, Y. Cerenius, J.C. Hanson, E. Dimasi, F. Besenbacher, T.R. Jensen, J. Phys. Chem. C 112 (2008) 1299–1303.

[32] F. Pendolino, P. Mauron, A. Borgschulte, J. Phys. Chem. C 113 (2009) 17231–17234.
[33] J.H. Her, M. Yousufuddin, W. Zhou, S.S. Jalisatgi, J.G. Kulleck, J.A. Zan, S.J. Hwang, R.C. Bowman, T.J. Uclovict, Inorg. Chem. 47 (2008) 9757–9759.
[34] H.D. Lutz, M. Schneider, Z. Naturforsch. (B) 45 (1990) 1543–1547.
[35] Y. Fukai, T. Haraguchi, H. Shinomiya, K. Mori, Scr. Mater. 46 (2002) 679–684.
[36] L. Mosegaard, B. Moller, J.E. Jorgensen, U. Bosenberg, M. Dornheim, J.C. Hanson, Y. Cerenius, G. Walker, H.J. Jakobsen, F. Besenbacher, T.R. Jensen, J. Alloys Compd. 446 (2007) 301–305.
[37] S.I. Orimo, Y. Nakamori, N. Ohba, K. Miwa, M. Aoki, S. Towata, A. Züttel, Appl. Phys. Lett. 89 (2006) 021920.
[38] D. Reed, D. Book, Mater. Res. Soc. Symp. Proc. 1216 (2010).
[39] N. Mironova-Ulmane, A. Kuzmin, M. Grube, J. Alloys Compd. 480 (2009) 97–99.
[40] F. Buciuman, F. Patcas, R. Craciun, D.R.T. Zahn, Phys. Chem. Chem. Phys. 1 (1999) 185–190.
[41] W. Sun, Y. Du, S. Liu, B. Huang, C. Jiang, J. Phase Equilib. 31 (2010) 357–364.